# Chronology of Quaternary glaciations in East Africa

Timothy M. Shanahan *, Marek Zreda

*Department of Hydrology and Water Resources, University of Arizona, Tucson, AZ 85721, USA*

## Abstract

A new glacial chronology for equatorial East Africa is developed using in situ cosmogenic $^{36}Cl$ measured in 122 boulders from moraines on Mount Kenya and Kilimanjaro. The oldest deposits sampled on Kilimanjaro yield a limiting $^{36}Cl$ age of $> 360$ calendar kyr (all $^{36}Cl$ ages are in calendar years, cal. kyr or cal. yr). On Mount Kenya, the oldest moraines give ages of 355–420 kyr (Liki I) and 255–285 kyr (Teleki). Given the uncertainty in our $^{36}Cl$ ages, the Liki I moraine may correspond to either marine isotope stage 10 or 12, whereas the Teleki moraine correlates with stage 8. There is no evidence for stage 6 on either mountain. The Liki II moraines on Mt. Kenya and moraines of the Fourth Glaciation on Kilimanjaro give ages of $28 \pm 3$ kyr and $20 \pm 1$ kyr, respectively. They represent the last glacial maximum (LGM) and correlate with stage 2 of the marine isotope record. A series of smaller moraines above the LGM deposits record several readvances that occurred during the late glacial. On Mt. Kenya, these deposits date to $14.6 \pm 1.2$ kyr (Liki IIA), $10.2 \pm 0.5$ kyr (Liki III), $8.6 \pm 0.2$ kyr (Liki IIIA) and $\sim 200$ yr (Lewis); the corresponding deposits on Kilimanjaro have mean ages of $17.3 \pm 2.9$ kyr (Fourth Glaciation–Saddle), $15.8 \pm 2.5$ kyr (Little Glaciation–Saddle), and $13.8 \pm 2.3$ kyr (Fourth Glaciation–Kibo). These data indicate that the climate of the tropics was extremely variable at the end of the last glacial cycle. © 2000 Elsevier Science B.V. All rights reserved.

*Keywords:* Quaternary; glaciation; East Africa; chronology

## 1. Introduction

Tropical East Africa is one of three places on the equator with direct glacial–geomorphologic evidence of former, expanded glaciers; the other two are in South America and New Guinea. The age and extent of moraines deposited by these glaciers provide a record of the magnitude and timing of climate change in the tropics. On Mount Kenya and Kilimanjaro, these glacial deposits have been described in detail [1,2]. However, the construction of an accurate glacial chronology for these mountains has been hindered by difficulties in the absolute dating of the deposits. These difficulties are primarily due to the paucity of datable material and the limited time range of applicability of available methods. In this study, we used cosmogenic $^{36}Cl$ to determine surface exposure ages of moraines on Mt. Kenya and Kilimanjaro (Fig. 1) and to reconstruct the timing and extent of glaciations in tropical East Africa. Development of a reliable glacial chronology will aid in our efforts to correlate the terrestrial record of glaciations in East Africa with other records of

* Corresponding author. Tel.: +1-520-621-4072;
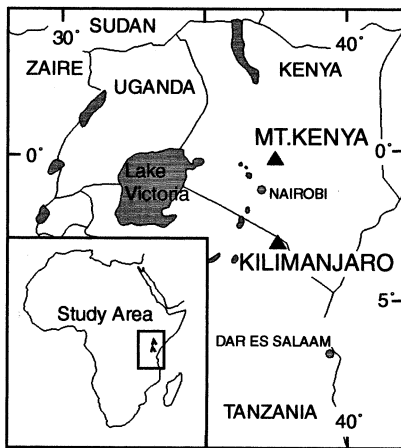Fax: +1-520-621-1422; E-mail: shanahan@hwr.arizona.edu

Fig. 1. Locations of Kilimanjaro and Mt. Kenya in East Africa.

paleoclimate, such as pollen, sea sediments and ice cores.

## 2. Prior work

### 2.1. Mt. Kenya

Glacial deposits on Mt. Kenya are present from 4600 m to less than 2900 m. Figs. 2a–d are comprehensive maps of these glacial deposits, modified from previous studies [1,3]. Seven stages of glacial moraines have been identified (from oldest to youngest): Gorges, Lake Ellis, Naro Moru, Teleki, Liki (I, II, III), Tyndall and Lewis [1]. The chronology for the oldest deposits (Gorges, Lake Ellis, Naro Moru and Teleki) is based on paleomagnetic data and stratigraphic relationships [1]. Age estimates for the Liki (I, II, III) deposits have been hindered by the lack of associated datable material and problems with obtaining sufficient organic material from core bottoms [4,5]. The chronology for neoglacial deposits is known from historical records (Lewis) and lichenometry (Tyndall) [1].

### 2.2. Kilimanjaro

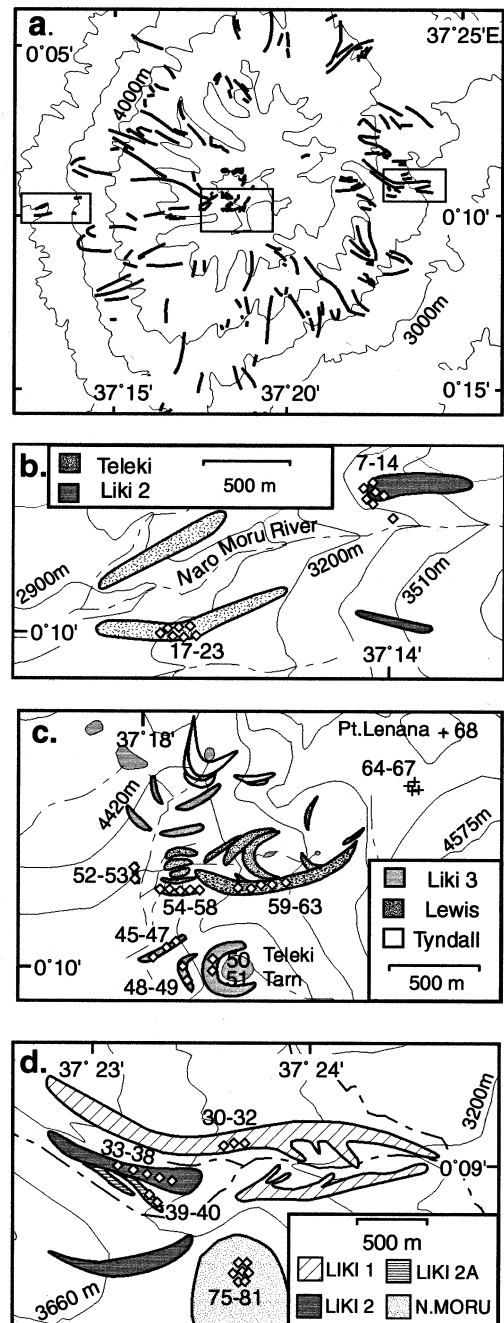Downie and Wilkinson [2] mapped the glacial deposits on Kilimanjaro and developed a rough



Fig. 2. (a) Moraines on Mt. Kenya. Solid lines indicate moraines mapped from aerial photographs. Boxes indicate location of study areas magnified in b–d. Maps of study areas adapted from Mahaney [1] with moraines and sample locations: (b) lower Teleki Valley; (c) upper Teleki Valley; (d) Gorges Valley.

Fig. 3. (a) Moraines on Kilimanjaro. Solid lines indicate moraines mapped from aerial photographs. Boxes indicate location of study areas magnified in b–d. Maps of study areas with moraines and sample locations: (b) east slopes of Kibo Peak; (c) the Saddle; (d) south slopes of Mawenzi Peak.

→



chronology for the oldest glaciations based on volcanic rocks associated with glacial deposits. Their mapping was later confirmed using aerial photographs [3]. Four major Pleistocene glaciations are identified (from oldest to youngest): the First, the Second, the Third and the Fourth (Main). Of these, only the Main Glaciation is associated with a system of moraines. The absence of volcanics associated with the Main Glaciation has left its age in question. Two Holocene glaciations were also identified: the Recent and the Little, both of which form moraines inside those of the Main Glaciation. No chronological control is available for the younger deposits. Maps of the deposits based upon field observations, aerial photographs and previous studies [2,3] are shown in Fig. 3a–d.

## 3. Methods

### 3.1. Sampling and analytical procedures

Sampling on Mt. Kenya was conducted in east–west trending valleys, which were reported [1] to have the most favorable deposits for surface exposure dating (Fig. 2). On Kilimanjaro, sampling concentrated on the southern slopes of Mawenzi and on the Saddle between Kibo and Mawenzi (Fig. 3). The primary criteria used in selection of samples were boulder size, position on the moraine crest and surface character. To minimize the effect of landform erosion and snow cover on the exposure history of the samples, we collected from the tops of the largest boulders located along moraine crests. Boulders were also selected on the basis of surface preservation and glacial character (shape and the presence of striae or polish).

Whole-rock samples were ground to a size fraction 0.25–1.00 mm and leached in 5% $HNO_3$ to remove meteoric Cl and any secondary carbonates
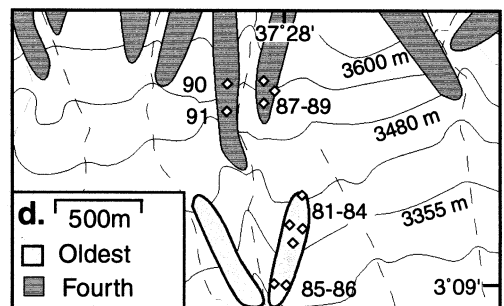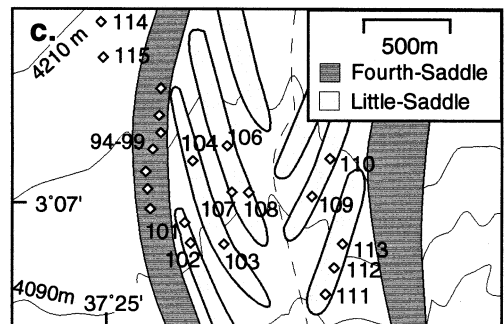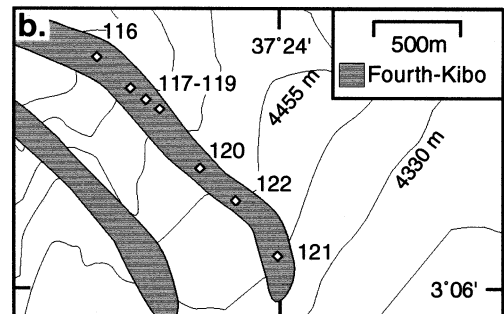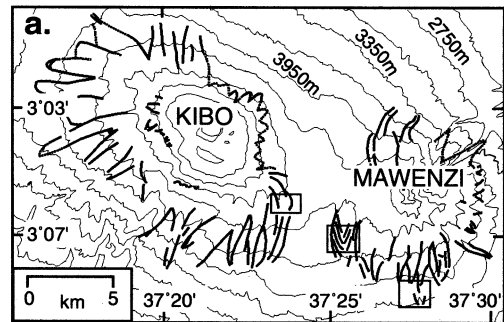
Table 1
Data for $^{36}Cl$ ages of old glaciations

| Sample ID | $^{36}Cl/Cl$ (10$^{-15}$) | Cl (ppm) | $P$ ($^{36}Cl/(g\ yr)$) | Age (kyr) |
|---|---|---|---|---|
| *Oldest Glaciation, South Mawenzi* | | | | |
| MP-81 | 6 640 ± 130 | 41.0 ± 2.1 | 45 | 117.0 ± 3.0 |
| MP-82 | 20 600 ± 800 | 26.4 ± 0.6 | 38 | 355.0 ± 22.0 |
| MP-83 | 6 460 ± 260 | 22.4 ± 2.2 | 36 | 74.0 ± 3.0 |
| MP-84 | 14 360 ± 290 | 24.2 ± 3.7 | 40 | 200.0 ± 5.0 |
| MP-85 | 8 550 ± 170 | 45.1 ± 0.1 | 40 | 205.0 ± 5.0 |
| MP-86[a] | 25 390 ± 590 | 25.5 ± 0.6 | 32 | 663.0 ± 37.0 |
| Coefficient of variation | | | | 0.80 |
| Landform age | | | | **> 360** |
| *Gorges Valley: Liki I* | | | | |
| GV-30 | 3 500 ± 120 | 670.0 ± 63.3 | 98 | 432.0 ± 26.0 |
| GV-31 | 2 490 ± 80 | 1 177.5 ± 80.4 | 169 | 329.0 ± 16.0 |
| GV-32 | 2 620 ± 90 | 1 423.1 ± 89.1 | 202 | 383.0 ± 22.0 |
| Coefficient of variation | | | | 0.135 |
| Landform age | | | | **355–420**[b] |
| *Teleki Valley: Teleki* | | | | |
| TV-17 | 1 810 ± 70 | 768.8 ± 11.5 | 124 | 243 ± 13 |
| TV-18[a] | 2 820 ± 90 | 837.2 ± 36.6 | 129 | 531 ± 35 |
| TV-19 | 1 940 ± 70 | 667.5 ± 25.4 | 111 | 255 ± 13 |
| TV-20 | 2 180 ± 48 | 652.7 ± 28.2 | 109 | 300 ± 10 |
| TV-21 | 1 641 ± 49 | 927.8 ± 58.5 | 141 | 231 ± 10 |
| TV-22 | 5 070 ± 140 | 58.4 ± 5.5 | 43 | 134 ± 5 |
| TV-23 | 7 200 ± 280 | 53.5 ± 3.5 | 40 | 200 ± 10 |
| Coefficient of variation | | | | 0.247 |
| Landform age | | | | **255–285**[b] |
| *Gorges Valley: Naro Moru till* | | | | |
| GV-74 | 503 ± 22 | 497 ± 1.4 | 121 | 33 ± 2 |
| GV-75 | 476 ± 15 | 930 ± 45.1 | 194 | 37 ± 1 |
| GV-76 | 1 278 ± 51 | 115 ± 6.8 | 69 | 36 ± 2 |
| GV-77 | 666 ± 4.2 | 1 136 ± 56.1 | 238 | 54 ± 0.3 |
| GV-78 | 1 029 ± 39 | 639 ± 38.9 | 163 | 71 ± 3 |
| GV-79 | 1 043 ± 43 | 257 ± 10.8 | 100 | 46 ± 2 |
| GV-80 | 723 ± 31 | 1 106 ± 58.6 | 229 | 60 ± 3 |
| GV-81 | 1 172 ± 51 | 1 171 ± 81.1 | 251 | 101 ± 5 |
| Coefficient of variation | | | | 0.41 |
| Landform age | | | | **55 ± 23** |
| *Teleki Valley: Liki II* | | | | |
| TV-7 | 1 520.0 ± 60 | 806 ± 15.7 | 201 | 114.0 ± 5 |
| TV-8 | 1 770.0 ± 60 | 831 ± 0.2 | 210 | 135.0 ± 6 |
| TV-9 | 746.0 ± 30 | 1 039 ± 10.2 | 215 | 62.0 ± 3 |
| TV-10 | 1 027.0 ± 37 | 1 123 ± 0.1 | 238 | 87.0 ± 4 |
| TV-11 | 1 007.0 ± 20 | 211 ± 0.5 | 86 | 42.0 ± 0.9 |
| TV-12 | 367.0 ± 14 | 1 695 ± 36.0 | 304 | 33.0 ± 1 |
| TV-13 | 608.0 ± 24 | 1 744 ± 0.7 | 322 | 56.0 ± 2 |
| TV-14 | 239.0 ± 8 | 943.8 ± 3.9 | 171 | 19.2 ± 0.7 |
| TV-15 | 283.0 ± 8 | 1 139 ± 15.9 | 209 | 23.0 ± 0.7 |
| TV-16 | 1 294.0 ± 39 | 373 ± 5.7 | 121 | 71.0 ± 2 |
| Coefficient of variation | | | | 0.60 |
| Landform age | | | | **64 ± 40** |

Ages > 20 kyr rounded to nearest 1 kyr.
[a]Sample excluded from consideration.
[b]Age estimated using erosion model.

from pore spaces. Cl was extracted by dissolving in a mixture of hot HF and $HNO_3$ and precipitated as AgCl for $^{36}Cl$ analysis by accelerator mass spectrometry [6] at PRIME Lab, Purdue University. Major elements were measured by prompt gamma spectroscopy, U and Th by neutron activation analysis and total Cl by specific ion electrode [7].

### 3.2. Principles

Production of $^{36}Cl$ occurs via interactions between cosmic-ray neutrons and muons with $^{39}K$, $^{40}Ca$ and $^{35}Cl$ in landforms exposed at the Earth's surface. Because the depth dependence of the production and decay rates for $^{36}Cl$ are known, the time of deposition of the surface can be determined. The principles of cosmogenic dating of landforms have been described elsewhere [8,9]. The utility of cosmogenic dating techniques for developing glacial chronologies has been demonstrated by numerous workers [10–19].

Calculations of the elevation and latitude dependence of $^{36}Cl$ production rates were performed according to Lal [9]. Corrections for topographic shielding were made using the formulation of Zreda and Phillips [20]. The production rate of $^{36}Cl$ due to thermal and epithermal neutron absorption by $^{35}Cl$ was calculated using the method outlined in Liu et al. [21]. Age calculations were performed using the computer program CHLOE [22].

We used the $^{36}Cl$ production parameters determined by Phillips et al. [23]: $73.3 \pm 4.9$ atoms $^{36}Cl$ (g Ca)$^{-1}$ yr$^{-1}$, $154 \pm 10$ atoms $^{36}Cl$ (g K)$^{-1}$ yr$^{-1}$ and $586 \pm 40$ fast neutrons (g air)$^{-1}$ yr$^{-1}$. Though other workers have determined different production rates [24,25], there is no indication that they are more accurate than those of Phillips et al. [23]. Random errors associated with the calibration should be smaller than 10% [23] and overall random errors for moraine ages should not exceed 15% [17]. Uncertainties related to temporal variability in production rates are less well understood. Because these variations are significant at low-latitude sites, these effects are discussed in greater detail below.

Analytical error is primarily a function of uncertainties in the measurements of $^{36}Cl/Cl$ and of total Cl. The error associated with AMS measurements was on average 4.9%, though some samples had errors as high as 28.6% or as low as 0.6%. Uncertainty in measurements of total Cl ranged from 0.0% (based on three identical measurements) to 16.7% with a mean of 4.6%. The total analytical error for the age of each sample was determined using Monte Carlo simulation. Ten thousand ages were generated assuming normal distributions of possible total Cl and $^{36}Cl/Cl$ values. Individual sample standard deviations were then calculated based upon the range of possible ages produced by the simulation. Errors reported in Tables 1 and 2 reflect only the Monte Carlo-derived uncertainties.

### 3.3. Corrections for temporal variability in cosmic radiation

Variations in the flux of cosmic radiation result in changes in cosmogenic production rates over time. These variations are a function of (i) changes in the intensity of galactic cosmic rays, (ii) changes in solar activity and (iii) changes in the strength of the geomagnetic field. Because variations in the first two factors are too long and too short, respectively, to significantly affect production rates for time scales of interest (ca. 10–700 kyr), we consider only the effect of variations in the geomagnetic field strength on production rates.

Cosmic rays consist primarily of charged protons and alpha particles. Those with sufficient energies are able to penetrate the geomagnetic field and produce cosmogenic nuclides. Any variations in the strength of the geomagnetic field over time result in changes in the cosmic-ray flux and changes in production rates. Because the magnetic field has a greater influence on the cosmic-ray flux at the equator than at the poles, the effect of variations in the field strength on production rates is larger at low latitudes. Production rates determined at middle and high latitudes, where the effect of the geomagnetic field is negligible [23], need to be modified to account for variations in the magnetic field, especially for applications at low latitudes. Recent paleomagnetic records [26] indicate that variations in the geomagnetic field

Table 2
Data for $^{36}$Cl ages of young glaciations and stromatolites

| Sample ID | $^{36}$Cl/Cl | Cl | $P$ | Age (kyr) | |
|---|---|---|---|---|---|
| | $(10^{-15})$ | (ppm) | $(^{36}$Cl/(g yr)) | 0 mm kyr$^{-1}$ | 2 mm kyr$^{-1}$ |
| *Liki II, Gorges Valley, Mt. Kenya* | | | | | |
| GV-33 | $425 \pm 21$ | $21.0 \pm 45.7$ | 110 | $32 \pm 2$ | $28 \pm 2$ |
| GV-34 | $751 \pm 35$ | $35.0 \pm 4.5$ | 44 | $24 \pm 1$ | $23 \pm 1$ |
| GV-35 | $293 \pm 13$ | $13.0 \pm 17.2$ | 189 | $27 \pm 1$ | $23 \pm 1$ |
| GV-36 | $2\,830 \pm 140$ | $140.0 \pm 0.2$ | 45 | $28 \pm 1$ | $30 \pm 1$ |
| GV-37 | $316 \pm 12$ | $12.0 \pm 6.2$ | 152 | $28 \pm 1$ | $24 \pm 1$ |
| GV-38 | $1\,354 \pm 55$ | $55.0 \pm 2.4$ | 46 | $32 \pm 1$ | $31 \pm 1$ |
| Landform age | | | | **28 ± 3** | |
| *Main Glaciation, Mawenzi, Kilimanjaro* | | | | | |
| MP-87 | $841 \pm 38$ | $59.8 \pm 6.2$ | 43 | $20 \pm 1$ | $20 \pm 1$ |
| MP-88[a] | $8\,870 \pm 340$ | $21.0 \pm 3.5$ | 34 | $103 \pm 5$ | $119 \pm 5$ |
| MP-89[a] | $1\,071 \pm 51$ | $68.4 \pm 1.2$ | 45 | $28 \pm 1$ | $28 \pm 1$ |
| MP-90[a] | $474 \pm 19$ | $103.7 \pm 1.3$ | 51 | $16.4 \pm 0.7$ | $16.1 \pm 0.7$ |
| MP-91 | $1\,270 \pm 50$ | $33.3 \pm 3.8$ | 37 | $19.7 \pm 0.8$ | $19.8 \pm 0.8$ |
| MP-92 | $1\,230 \pm 34$ | $40.5 \pm 0.7$ | 42 | $21 \pm 1$ | $21 \pm 1$ |
| Landform age | | | | **20 ± 1** | |
| *Main Glaciation, Saddle, Kilimanjaro* | | | | | |
| MP-94 | $450 \pm 70$ | $194.7 \pm 0.6$ | 31 | $17.5 \pm 2.9$ | $16.7 \pm 2.9$ |
| MP-95 | $500 \pm 21$ | $150.1 \pm 0.9$ | 24 | $16.7 \pm 0.7$ | $16.1 \pm 0.7$ |
| MP-96 | $569 \pm 25$ | $143.5 \pm 10.8$ | 22 | $19.1 \pm 0.9$ | $18.5 \pm 0.9$ |
| MP-97 | $405 \pm 16$ | $181.8 \pm 0.7$ | 28 | $15.8 \pm 0.7$ | $15.2 \pm 0.7$ |
| MP-98 | $428 \pm 29$ | $156.7 \pm 3.3$ | 24 | $15.4 \pm 1.1$ | $14.9 \pm 1.1$ |
| MP-99 | $587 \pm 25$ | $179.1 \pm 6.5$ | 28 | $23 \pm 1$ | $22 \pm 1$ |
| MP-100 | $347 \pm 14$ | $192.8 \pm 5.0$ | 31 | $13.6 \pm 0.6$ | $13.2 \pm 0.6$ |
| Landform age | | | | **17.3 ± 2.9** | |
| *Little Glaciation, Saddle, Kilimanjaro* | | | | | |
| MP-101 | $904 \pm 41$ | $72.4 \pm 0.4$ | 71 | $15.7 \pm 0.7$ | $15.7 \pm 0.7$ |
| MP-102 | $689 \pm 33$ | $101.5 \pm 5.5$ | 74 | $15.9 \pm 0.8$ | $15.7 \pm 0.8$ |
| MP-103 | $415 \pm 19$ | $138.2 \pm 8.9$ | 71 | $13.5 \pm 0.7$ | $13.1 \pm 0.7$ |
| MP-104 | $377 \pm 16$ | $208.3 \pm 14.9$ | 83 | $15.7 \pm 0.7$ | $15.0 \pm 0.7$ |
| MP-106 | $905 \pm 33$ | $88.1 \pm 0.9$ | 72 | $19.0 \pm 0.7$ | $18.8 \pm 0.7$ |
| MP-107 | $470 \pm 22$ | $188.5 \pm 3.3$ | 80 | $18.6 \pm 0.9$ | $17.8 \pm 0.9$ |
| MP-108 | $471 \pm 20$ | $158.7 \pm 0.9$ | 77 | $16.2 \pm 0.7$ | $15.7 \pm 0.7$ |
| MP-109 | $605 \pm 28$ | $116.4 \pm 8.6$ | 67 | $17.7 \pm 0.9$ | $17.2 \pm 0.9$ |
| MP-110 | $365 \pm 26$ | $222.0 \pm 5.1$ | 94 | $14.4 \pm 1.1$ | $13.9 \pm 1.1$ |
| MP-111 | $512 \pm 14$ | $100.0 \pm 0.0$ | 67 | $12.7 \pm 0.4$ | $12.4 \pm 0.4$ |
| MP-112 | $490 \pm 140$ | $183.5 \pm 10.6$ | 78 | $19.2 \pm 5.8$ | $18.4 \pm 5.8$ |
| MP-113 | $298 \pm 10$ | $203.2 \pm 5.5$ | 86 | $11.5 \pm 0.4$ | $11.1 \pm 0.4$ |
| Landform age | | | | **15.8 ± 2.5** | |
| *Fourth Glaciation, Kibo Peak, Kilimanjaro* | | | | | |
| KB-116$_{BR}$ | $777 \pm 35$ | $175.7 \pm 13.9$ | 117 | $18.5 \pm 0.9$ | $17.7 \pm 0.9$ |
| KB-117$_{BR}$ | $1\,866 \pm 55$ | $83.1 \pm 2.8$ | 94 | $28 \pm 1$ | $28 \pm 1$ |
| KB-118$_{BR}$ | $1\,482 \pm 48$ | $78.7 \pm 2.6$ | 89 | $22 \pm 1$ | $22 \pm 1$ |
| KB-119 | $603 \pm 19$ | $120.8 \pm 3.7$ | 94 | $12.0 \pm 0.4$ | $11.7 \pm 0.4$ |
| KB-120 | $1\,166 \pm 53$ | $60.1 \pm 1.8$ | 78 | $14.8 \pm 0.7$ | $14.7 \pm 0.7$ |
| KB-121 | $596 \pm 26$ | $176.4 \pm 3.0$ | 97 | $16.8 \pm 0.8$ | $16.1 \pm 0.8$ |
| KB-122 | $445 \pm 17$ | $178.9 \pm 3.3$ | 97 | $12.1 \pm 0.5$ | $11.8 \pm 0.5$ |
| Landform age | | | | **13.8 ± 2.3** | |

Table 2 (*continued*)

| Sample ID | $^{36}$Cl/Cl (10$^{-15}$) | Cl (ppm) | $P$ ($^{36}$Cl/(g yr)) | Age (kyr) 0 mm kyr$^{-1}$ | 2 mm kyr$^{-1}$ |
|---|---|---|---|---|---|
| *Liki IIA, Gorges Valley, Mt. Kenya* | | | | | |
| GV-39 | 170 ± 11 | 1 040.4 ± 45.8 | 155 | 13.9 ± 0.9 | 12.7 ± 0.9 |
| GV-40 | 191 ± 11 | 891.9 ± 62.6 | 140 | 15.5 ± 0.9 | 14.1 ± 0.9 |
| Landform age | | | | **14.6 ± 1.2** | |
| *Liki III boulders, Gorges Valley, Mt. Kenya* | | | | | |
| GV-69 | 1 171 ± 39 | 32.8 ± 0.0 | 59 | 10.8 ± 0.4 | 10.8 ± 0.4 |
| GV-70$_{BR}$ | 349 ± 15 | 560.0 ± 12.7 | 162 | 18.4 ± 0.8 | 16.8 ± 1 |
| GV-71 | 1 343 ± 50 | 40.5 ± 0.1 | 63 | 14.5 ± 0.6 | 14.6 ± 0.6 |
| GV-72 | 3 170 ± 110 | 10.8 ± 0.5 | 42 | 13.7 ± 0.5 | 13.9 ± 0.5 |
| GV-73$_{BR}$ | 3 360 ± 120 | 12.2 ± 0.1 | 42 | 16.6 ± 0.6 | 16.9 ± 0.6 |
| Landform age | | | | **14.1 ± 0.6** | |
| *Liki III, Teleki Valley, Mt. Kenya* | | | | | |
| TV-45 | 222 ± 12 | 447.7 ± 17.3 | 128 | 10.4 ± 0.6 | 9.9 ± 0.6 |
| TV-46 | 363 ± 16 | 192.9 ± 5.1 | 90 | 10.9 ± 0.5 | 10.6 ± 0.5 |
| TV-47 | 139 ± 9 | 1 044 ± 29.9 | 163 | 9.5 ± 0.6 | 8.9 ± 0.6 |
| TV-48 | 286 ± 14 | 211.0 ± 2.5 | 91 | 10.5 ± 0.5 | 10.1 ± 0.5 |
| TV-49[a] | 227 ± 12 | 469.8 ± 22.5 | 120 | 13.1 ± 0.7 | 12.3 ± 0.7 |
| TV-50 | 1 680 ± 70 | 17.4 ± 1.7 | 50 | 9.9 ± 0.4 | 10.0 ± 0.4 |
| TV-51 | 1 662 ± 59 | 18.6 ± 1.6 | 51 | 10.1 ± 0.4 | 10.2 ± 0.4 |
| Landform age | | | | **10.2 ± 0.5** | |
| *Liki IIIA, Teleki Valley, Mt. Kenya* | | | | | |
| TV-52 | 907 ± 38 | 38.3 ± 0.4 | 53 | 10.4 ± 0.5 | 10.5 ± 0.5 |
| TV-53 | 1 350 ± 60 | 20.2 ± 0.3 | 53 | 8.4 ± 0.4 | 8.4 ± 0.4 |
| TV-54 | 661 ± 27 | 33.6 ± 1.6 | 59 | 5.9 ± 0.3 | 6.0 ± 0.3 |
| TV-55 | 250 ± 11 | 238.3 ± 9.7 | 81 | 11.2 ± 0.5 | 10.9 ± 0.5 |
| GV-56 | 167 ± 7 | 663.7 ± 26.2 | 149 | 8.8 ± 0.4 | 8.4 ± 0.4 |
| TV-57 | 175 ± 7 | 651.8 ± 20.6 | 143 | 11.9 ± 0.5 | 11.2 ± 0.5 |
| TV-58 | 806 ± 40 | 33.0 ± 0.1 | 45 | 8.6 ± 0.5 | 8.6 ± 0.5 |
| Landform age | | | | **8.6 ± 0.2** | |
| *Lewis, Teleki Valley, Mt. Kenya* | | | | | |
| TV-59 | 52 ± 5 | 180.7 ± 3.4 | 299 | 0.10 ± 0.01 | 0.10 ± 0.01 |
| TV-60 | 74 ± 4 | 179.8 ± 1.6 | 268 | 0.33 ± 0.02 | 0.33 ± 0.02 |
| TV-61 | 166 ± 7 | 132.7 ± 10.0 | 227 | 1.2 ± 0.05 | 1.2 ± 0.05 |
| TV-62 | 55 ± 5 | 209.5 ± 12.3 | 408 | 0.20 ± 0.02 | 0.20 ± 0.02 |
| TV-63 | 73 ± 6 | 99.8 ± 9.3 | 231 | 0.20 ± 0.02 | 0.20 ± 0.02 |
| Landform age | | | | **0.21 ± 0.21** | |
| *Late Glacial deposits, Mt. Kenya* | | | | | |
| TV-64 | 60 ± 6 | 196.0 ± 5.5 | 367 | 0.15 ± 0.02 | 0.15 ± 0.02 |
| TV-65 | 431 ± 21 | 22.9 ± 2.7 | 241 | 0.63 ± 0.03 | 0.63 ± 0.03 |
| TV-66 | 57 ± 5 | 28.8 ± 3.9 | 231 | 0.03 ± 0.00 | 0.03 ± 0.00 |
| TV-67 | 45 ± 6 | 55.4 ± 3.0 | 257 | **0.00 ± 0.00** | 0.00 ± 0.00 |
| *Point Lenana, striated bedrock, Mt. Kenya* | | | | | |
| PL-68 | 114 ± 5 | 1 140.2 ± 63.7 | 337 | 4.1 ± 0.2 | 4.0 ± 0.2 |
| *Gorges landform, Gorges Valley, Mt. Kenya* | | | | | |
| GV-26[a] | 178 ± 8 | 446.1 ± 1.4 | 56.7 | 22 ± 1 | 20 ± 1 |
| GV-27 | 159 ± 8 | 51.6 ± 1.2 | 21.8 | 5.9 ± 0.3 | 5.9 ± 0.3 |
| GV-28 | 74 ± 10 | 361.9 ± 4.1 | 50.1 | 7.6 ± 1.1 | 7.3 ± 1.1 |
| GV-29 | 83 ± 8 | 675.1 ± 52.3 | 81.2 | 6.3 ± 0.6 | 6.0 ± 0.6 |
| Landform age | | | | **6.6 ± 0.9** | |

Table 2 (*continued*)

| Sample ID | $^{36}Cl/Cl$ | Cl | $P$ | Age (kyr) | |
|---|---|---|---|---|---|
| | $(10^{-15})$ | (ppm) | $(^{36}Cl/(g\ yr))$ | 0 mm kyr$^{-1}$ | 2 mm kyr$^{-1}$ |
| **Ages of stromatolites** | | | | | |
| *Lake Tauca, Bolivia* | | | | | |
| CH-47 | $2\,400 \pm 100$ | $65.8 \pm 1.9$ | 186 | $14.6 \pm 0.6$ | $14.8 \pm 1$ |
| *Lake Magadi, Kenya* | | | | | |
| KE-1-ML | $267 \pm 17$ | $41.8 \pm 3.5$ | 19 | $12.5 \pm 0.8$ | $12.6 \pm 1$ |
| KE-3-ML | $509 \pm 25$ | $22.5 \pm 1.3$ | 19 | $12.9 \pm 0.7$ | $13.1 \pm 1$ |
| KE-4-ML | $726 \pm 34$ | $16.2 \pm 1.4$ | 21 | $12.2 \pm 0.6$ | $12.4 \pm 1$ |
| KE-5-ML[a] | $475 \pm 44$ | $20.2 \pm 0.2$ | 22 | $9.2 \pm 0.9$ | $9.3 \pm 1$ |
| Stromatolite age | | | | **$12.5 \pm 0.4$** | |

[BR], Bedrock sample excluded from consideration.

Ages > 20 kyr rounded to nearest 1 kyr.

[a]Sample outlier excluded from consideration.

strength should average out over times longer than about 50 kyr.

To account for the effect of temporal changes in the geomagnetic field on cosmogenic nuclide production, production rates were scaled using a geomagnetic correction factor. This factor was based on the theory that each geomagnetic latitude has an associated effective vertical cutoff rigidity. Only those cosmic-ray particles with energies greater than this rigidity can pass through the magnetic field and enter the Earth's atmosphere. The cutoff rigidity ($R$) can be calculated for any latitude using the following relation: $R = 14.9(M/M_0)\ \cos^4\ \lambda$, where $\lambda$ is the geomagnetic latitude and $M/M_0$ is the relative strength of the geomagnetic dipole [27]. For times when the geomagnetic field was reduced ($M/M_0 < 1.0$), a new effective rigidity and a corresponding geomagnetic latitude can be calculated. Then, an adjusted production rate for the site can be determined using the scaling factors of Lal [9]. For situations of increased magnetic field strength ($M/M_0 > 1.0$), it is impossible to calculate an effective latitude because magnetic field strength is maximized at the equator, where $M/M_0 = 1.0$. In this case, we used the approximation: $Q/Q_0 = (M/M_0)^{-0.5}$, where $Q$ is the corrected production rate and $Q_0$ is the production rate corresponding to $M_0$ [28].

The 200 kyr relative magnetic intensity record (SINT-200) [26] was used as a record of past magnetic field variations. SINT-200 is a composite stack of 17 marine sediment records of paleoin-

tensity collected from around the world. Although paleomagnetic data from sources like lava flows and archeomagnetic studies are preferred to sediment records because they record absolute intensities, difficulties with development of continuous records and with chronological control limit the usefulness of these data. Previous studies (e.g. [29]) have shown that absolute records are generally in good agreement with marine sediment records. Furthermore, strong correlations between widely separated marine records as well as between marine records and $^{10}Be$ in sea sediments [30] indicate that marine records accurately record changes in the magnetic field.

The ratio $M/M_0$ is the relative strength of the geomagnetic dipole. At high latitudes, both $M$ and $M_0$ are essentially constant with time because variations in the field are negligible. For low latitudes, changes in the field are large and $M$ and $M_0$ must be calculated using a record of paleomagnetic field variations. Because changes in the field are cyclic over long times, the long-term average of the paleomagnetic record was used as an approximation for $M_0$. The parameter $M$ for each sample was calculated by integrating the magnetic field record of SINT-200 over the mean uncorrected landform age. Then, $M/M_0$ was used to calculate a new production rate, sample ages and an adjusted landform age. These values were used to produce a new $M$ and the procedure was iterated until the individual sample ages converged. Corrected ages using this procedure are reported in Tables 1 and 2.

## 3.4. Test of geomagnetic correction

To verify our method of geomagnetic correction, we collected samples from independently dated stromatolites at two low-latitude locations: paleolake Magadi in equatorial East Africa (2°S) and paleolake Tauca in Bolivia (19°S). The stromatolites from Lake Magadi form an almost continuous belt approximately 65 m above the current lake level, delineating the former extent of the lake. The western side of the lake is bounded by a large fault scarp on which the stromatolite belt is well-preserved and can easily be sampled. We identified and sampled four in situ stromatolite concretions. Previous studies of these stromatolites using ^{14}C yielded ages (converted to calendar years (cal. yr) using Stuiver et al. [31]) ranging from $7826 \pm 240$ to $14\,782 \pm 890$ cal. yr, with the majority of samples between 11\,000 and 13\,000 cal. yr [32].

One additional sample was collected from a large (1 m diameter) algal bioherm on a shoreline of paleolake Tauca. This sample provides a check of our paleomagnetic correction for a slightly higher latitude than that of the African samples. Previous studies using ^{14}C have yielded ages ranging from $14\,744 \pm 453$ to $16\,518 \pm 825$ cal. yr with a mean age of $15\,420 \pm 764$ cal. yr [33,34].

Fig. 4 shows the distributions of ^{14}C stromatolite ages (cal. kyr), uncorrected [36]Cl ages and corrected [36]Cl ages. The corrected [36]Cl ages agree at the 1σ level with ^{14}C ages for both Lake Magadi and paleolake Tauca. Uncorrected cosmogenic ages significantly underestimate the true age of the stromatolites. These results support our assumption that a correction for variations in the geomagnetic field is necessary and validate our method of adjusting low-latitude production rates.

Uncertainties associated with these magnetic corrections of production rates are difficult to evaluate for several reasons. With the exception of the stromatolites reported in this study, few other attempts have been made to quantify the effects of changes in the magnetic field strength at low latitudes using samples of known age [35,36]. Furthermore, little is known about the relationship between changes in magnetic field
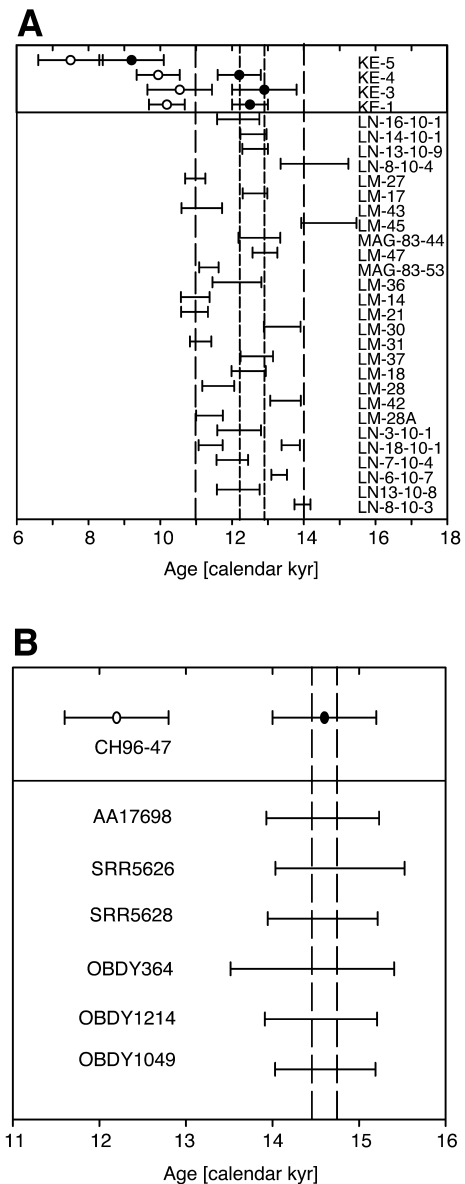


Fig. 4. Comparison between previously measured ^{14}C ages on (A) stromatolites from paleolake Magadi [32] and (B) stromatolites from paleolake Tauca (all ^{14}C ages converted to cal. yr using Stuiver et al. [31]), with [36]Cl ages corrected (filled circles) and uncorrected (empty circles) for the effect of changes in the geomagnetic field strength. Individual ^{14}C ages are shown as a range due to uncertainties in the conversion between radiocarbon and cal. yr.

strength and cosmogenic isotope production rates, particularly for equatorial regions where in the past field strengths were higher than anywhere today. Errors associated with these calculations cannot be assessed until more work in this area has been completed. Additional uncertainties arise from the inaccuracies of existing paleointensity records. Because the SINT-200 record is a composite of 17 marine sediment cores, it has errors associated with the analytical and chronological uncertainties from individual cores as well as uncertainties related to the stacking of the records. Despite these uncertainties, the SINT-200 record generally shows good consistency between the composite record and each individual record (mean correlation coefficient between SINT-200 and individual records = $0.6 \pm 0.16$ [26]) as well as with records of cosmogenic isotope production [30] and other records of magnetic field strength [37,38].

## 3.5. Effect of erosion on $^{36}$Cl ages

Additional uncertainty in surface exposure ages may result from post-depositional processes. Erosion of the soil matrix and degradation of boulder surfaces may result in apparent surface exposure ages different from the true age of the landform. Depending on the production mechanisms and the erosion rate, erosion of the boulder surface results in apparent ages that are either older or younger than the true age. For spallogenic nuclides, e.g. $^{10}$Be, $^{26}$Al, production rates decrease exponentially with depth. This results in apparent ages that always underestimate the true age of the surface. For nuclides which are also produced by neutron activation of Cl (e.g. $^{36}$Cl), ages may either under- or overestimate the true age. This is because the depth profile for production by neutron activation initially increases with depth before following an exponential decrease with depth.

Fig. 5 illustrates the theoretical distribution of apparent ages for two boulder chemistries as a function of surface erosion rate. For samples with low Cl, $^{36}$Cl production is controlled by spallation and therefore decreases exponentially with depth. For high Cl samples, in which neutron activation is a significant production mechanism,
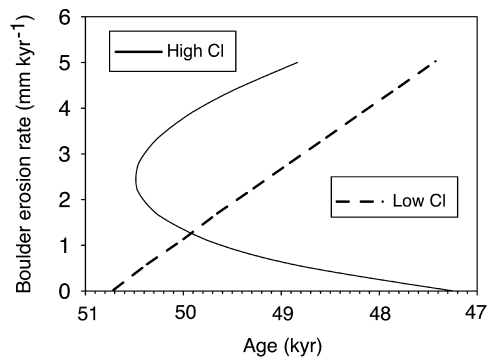


Fig. 5. Apparent cosmogenic ages as a function of boulder erosion rate for samples with high Cl (solid) and low Cl (dashed). High Cl sample has significant $^{36}$Cl production from neutron activation of $^{35}$Cl, while low Cl sample has mostly spallogenic $^{36}$Cl.

ages first increase with increasing erosion and then decrease with additional erosion. For young landforms, boulder erosion is a significant process affecting apparent boulder age. For older landforms, erosion of moraine matrix is more significant and will tend to dominate over the relatively slow erosion of the boulder surfaces. To illustrate the effect of boulder erosion on the apparent age of young samples, we report in Table 2 ages for zero erosion and for an erosion rate of 2 mm kyr$^{-1}$.

Although no independent information on erosion rates of boulder surfaces is available for these localities, we believe that a maximum erosion rate of 2 mm kyr$^{-1}$ is reasonable based upon field evidence and the results of studies from similar climates. Erosion rates of 0.2 mm kyr$^{-1}$ were previously estimated [17] for glacially deposited boulders in the Wind River Range, WY, USA, using the ratio of $^{36}$Cl to $^{10}$Be in the surfaces. Furthermore, Gosse and co-authors [13] argued that boulder erosion rates must be low in arid regions based upon observations of glacial striations and polish on boulders deposited 20 000 yr ago. Significantly higher erosion rates (2–8 mm kyr$^{-1}$) reported for bedrock in Africa [39,40] and Brazil [41] may not be applicable to our samples. Bedrock erosion rates may be higher than those of glacial deposits because they have longer exposures to weathering processes. In contrast, the process of glacial erosion preserves only the

hardest, most resistant rocks as large boulders. Surfaces pre-weathered prior to glacial plucking and erosion are more susceptible to disintegration during transport by the glacier. Furthermore, by sampling only the largest, freshest looking boulders, we preferentially select the boulders that are most resistant to weathering processes.

Erosion of soil matrix also results in apparent boulder ages that differ from the true landform age. Boulders deposited on the landform surface initially remain there whereas boulders deposited at some depth in the landform are gradually exposed with the removal of fine sediment and the progressive lowering of the landform surface. This results in an assemblage of boulders on the landform surface with a distribution of exposure histories and apparent ages that range from slightly older to younger than the age of the surface. By selecting the largest boulders ($>1$ m in most cases), located on or near to the moraine crest, we minimize the influence of gradual exposure on apparent boulder ages. For young landforms ($<30$ kyr), we assume that careful sampling makes the effect of soil erosion negligible when compared with other sources of uncertainty. This assumption is supported by the typically narrow distribution of apparent boulder ages for young landforms.

For older landforms, the distribution of boulder ages indicates that the effect of soil erosion is significant. A previous study [42] used Monte Carlo simulation of this process by generating a set of boulders randomly distributed in a gradually eroding landform. They found that the coefficient of variation for the simulated boulder ages is correlated with the erosion depth. Therefore, the distribution of apparent boulder ages and the mean apparent boulder age may be used to determine both the true age and the soil erosion rate for the landform.

In this study, this Monte Carlo simulation was expanded to include the effects of erosion of boulder surfaces. Ten thousand boulders were generated with chemistries randomly selected from the known chemical composition of boulders at the site. The initial depth of burial for the individual boulders was selected from a uniform distribution of depths between $x$, the actual height
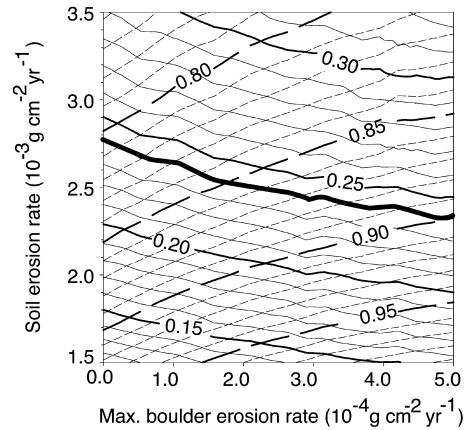


Fig. 6. Results of the soil–boulder erosion model for the Teleki moraine. Lines of constant apparent age/true age are dashed. Solid lines represent constant values for coefficient of variation. The Teleki moraine samples gave a coefficient of variation 0.24, which corresponds to apparent age/true age of 0.805–0.895.

of the boulder in the field, to some depth $x_{max}$, which is equal to the maximum erosion depth (for a particular erosion rate) subtracting the boulder height $x$. We assumed that across the landform, soil erosion rates are constant, even though initial boulder burial depths are not. Each boulder was also randomly assigned a boulder erosion rate from a lognormal distribution with values ranging from zero to an assigned maximum erosion rate ($x_{bmax}$). This distribution was used on the assumption that boulders are more likely to have boulder erosion rates that are closer to zero than they are to have erosion rates near the maximum. The simulation was run for all possible combinations of $x_{bmax}$ between zero and $5 \times 10^{-3}$ g cm$^{-2}$ yr$^{-1}$ (ca. 0–2 mm kyr$^{-1}$) and $x_{max}$ between zero and 2000 g cm$^{-2}$ (ca. 10 m). As mentioned above, the value for $x_{bmax}$ is based upon previously measured boulder erosion rates in arid regions [17]. The maximum soil erosion depth used in the model was large enough to include all possible matrix erosion rates that would produce the observed distribution of ages. For each combination of $x_{bmax}$ and $x_{max}$, a distribution of ages was determined and a coefficient of variation was calculated. The result is a distribution of all possible landform ages, dependent

upon the coefficient of variation, the soil erosion rate and the boulder erosion rate. A contour plot of the results for the Teleki moraine is shown in Fig. 6. Solid lines represent the coefficient of variation and dashed lines represent values of the ratio of the true age to apparent age (or constant age ratio). The intersections of the coefficient of variation line for the Teleki samples (0.247) and the lines of constant age ratio yield a range of true ages for all combinations of soil and boulder erosion rates. For a particular coefficient of variation, there is a small range of soil erosion rates associated with the possible range of true ages for the landform. For old landforms, we report the age as the range of possible true ages, and estimate the soil erosion rate using the range of all possible boulder erosion rates corresponding to experimental coefficient of variation.

Because this model assumes that soil erosion rate is constant in time and uniform across the same moraine, deviations from these conditions may lead to incorrect age estimates. A careful geomorphological examination of the deposits is critical to successful application of the model. Sampling should avoid areas with evidence of non-steady-state processes such as meltwater incision or deposition of boulders by successive glacial advances. Furthermore, the model should not be applied to deposits that may have undergone differential erosional and depositional processes during their history. In such cases, the observed coefficient of variation may be too large to be explained by steady-state erosion and therefore cannot be modeled using the techniques described above (for example, the Liki II moraine in Teleki Valley).

## 3.6. Prior exposure

We collected four samples of boulders and bed-

rock from the present margin of Lewis Glacier and five samples from the Lewis moraine in upper Teleki Valley to investigate the effect of prior exposure on surface exposure ages. Historical re-
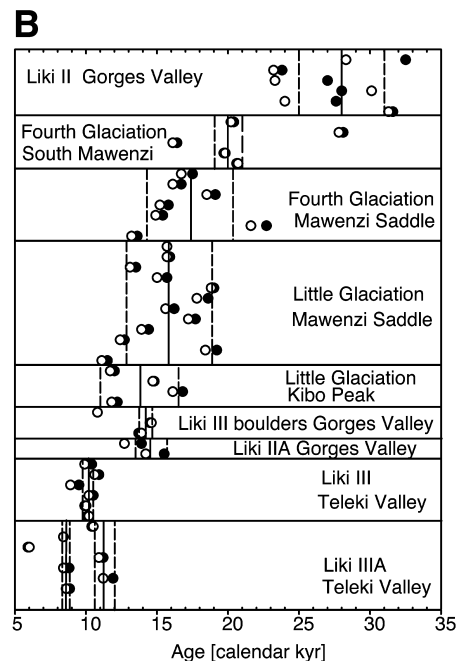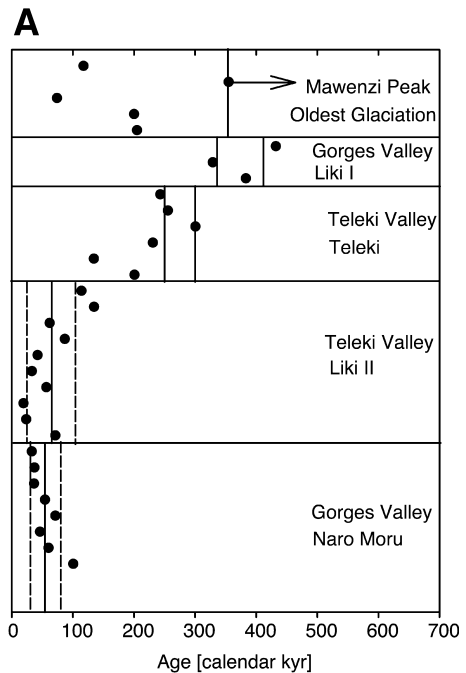


Fig. 7. Summary of apparent $^{36}Cl$ ages for (A) old and (B) young landforms on Mt. Kenya and Kilimanjaro. Filled circles represent ages for zero erosion, unfilled circles represent ages calculated with 2 mm kyr$^{-1}$ erosion rates. For old samples analyzed with the soil erosion model, we report a range of ages (solid lines). For young samples, we report the mean (solid line)±1σ (dashed lines) as the most probable age.

cords for the Lewis moraine indicate that it was deposited during the Little Ice Age [1]. Boulders collected from the present ice margin are thus expected to have a zero exposure age. With the exception of TV97-61 which gave an age of 1200 yr, the average age of the Lewis moraine was $210 \pm 90$ yr. The ice margin also had one outlier, TV97-65, with an age of 630 yr; other boulders yielded an age of $60 \pm 80$ yr. Even in the case of an anomalously old sample, such as TV97-61, prior exposure adds only 1000 yr, within the typical analytical uncertainty for most Pleistocene samples. The effect of prior exposure on sample ages is significant for very young samples (tens to hundreds of yr) and limits our ability to calculate landform ages in this time range. For older samples (thousands of yr), prior exposure should not pose a significant problem.

## 4. Results

The calculated surface exposure ages for the boulders used in this study are summarized in Tables 1 and 2 and Fig. 7. Full analytical results, with individual sample production rates and chemistry, are available as an **EPSL online Background dataset**[1] (Appendix A).

### 4.1. Mt. Kenya, Teleki Valley

We identified and sampled three distinct glacial landforms in Teleki Valley: the Teleki, the Liki III and the Lewis moraines of [1]. In addition, we collected samples from a Liki II moraine mapped by [1] and from glacially striated bedrock on Point Lenana. Our sampling locations for these moraines are indicated on Fig. 2.

The Teleki moraine is preserved as a broad, gently sloping ridge with several well-rounded boulders up to 2.0 m in diameter. Most boulders show indications of granular weathering and spalling. The age of the Teleki moraine was previously estimated at 150–300 kyr, based upon the high

percentage of clasts from the central volcanic plug present in the Teleki deposits [1]. We collected seven samples from boulders on the left lateral portion of the moraine near the meteorological station. Using the soil–boulder erosion model, we calculate a probable age range for the Teleki glaciation of 255–285 kyr, in agreement with previous estimates [1]. This result corresponds to a coefficient of variation of 0.247 and a soil erosion rate of 15.1–17.8 mm $kyr^{-1}$.

Several closely spaced moraine ridges at 4000 m, designated the Liki III moraines of Mahaney [1], are littered with boulders up to 1.0 m in diameter. Boulder surfaces are fresh and show no evidence of erosion. Previous radiocarbon dating of cores from glacially dammed lakes has provided minimum ages for Liki III deglaciation ranging from ca. 8.5 cal. kyr to ca. 15 cal. kyr [5] ($^{14}$C ages converted to calendar ages using Taylor [43]). Surface exposure ages give an average landform age of $10.2 \pm 0.5$ kyr for the Liki III moraines. Samples collected from the Liki IIIA moraine give an average age of $9.9 \pm 1.5$ kyr. The wide range of ages for the Liki IIIA compared with the Liki III moraine may indicate that erosion or prior exposure affected boulder ages. With the exception of the anomalously young TV-54 sample (5.9 kyr), boulder ages from this landform fall into two age groups: $11.2 \pm 0.8$ kyr and $8.6 \pm 0.2$ kyr. We suggest that perhaps the Liki IIIA landform is a composite of boulders deposited during the Liki III episode and boulders deposited during a second glacial advance at 8.6 kyr. Further studies of the deposits are needed to address this problem.

The surface mapped by Mahaney [1] as Liki II in Teleki Valley displays no clear moraine form (not recognizable on aerial photographs) and is confused by outcrops of bedrock observed in the field and on aerial photographs. Previous studies on buried paleosols associated with these deposits indicate that the Liki II glaciation may have begun around 30 cal. kyr [4]. We collected 10 samples from well-rounded, but heavily weathered boulders up to 2.0 m in diameter. These give a range of surface exposure ages from 19.0 kyr to 130 kyr (Fig. 7A). The coefficient of variation and mean apparent ages for these boulders are 0.60

---

[1] http//:www.elsevier.nl/locate/epsl; mirror site: http//:www.elsevier.com/locate/epsl

and 64 kyr, respectively. However, such high variability cannot be reproduced by the constant rate soil erosion model. This result can be explained by either the influence of non-uniform erosional processes or the deposition of boulders with significant prior exposure. Possible mechanisms include modification by meltwater incision or reworking by subsequent glacial or fluvial–glacial processes. These processes can also explain the lack of a well-defined landform shape and the presence of bedrock outcroppings. We conclude only that the age of the Liki II surface must lie between 10.2 kyr (Liki III in the upper valley) and 255–285 kyr (Teleki).

Polished and striated bedrock on Point Lenana (the third highest summit of Mt. Kenya, 4985 m) indicate that ice flowed to the east and southeast down Gorges and Hobley Valleys [1]. The striated surface gives an exposure age of 4.1 kyr. Because the bedrock is still covered by loose material in many places, this date should be considered a minimum deglaciation age for Point Lenana.

## 4.2. Mt. Kenya, Gorges Valley

On the eastern side of Mt. Kenya, in Gorges Valley (Fig. 2d), we identified and sampled two distinct Liki I and Liki II moraines [1]. We also collected samples from the Liki IIA moraine loops, the Naro Moru till, the Gorges moraine and from Liki III boulders and glacially scoured bedrock.

The Liki I moraine has a well-preserved shape with steep slopes that can be traced easily in the field and on aerial photographs in many valleys above 3200 m. Three very large (2.0–3.0 m diameter) boulders were identified on the Liki I moraine crest and sampled. No previous chronological control is available for the Liki I landform. Using the soil–boulder erosion model, we calculate a soil erosion rate of 5.2–6.7 mm kyr$^{-1}$ and estimate an age of between 420 and 355 kyr for the landform. The coefficient of variation for these three boulders, 0.135, is surprisingly small for a landform of such antiquity. The erosion rates are less than half those estimated for the western side of the mountain. This may be expected, given the well-preserved form of the Liki

I moraine compared with the subdued topography of the Teleki moraine. Observed vegetation patterns corresponding to moist and semi-arid microclimates on the east and west sides of the mountain, respectively, lend further support to these calculated erosion rates.

The Liki II moraine in Gorges Valley [1] is preserved as a sharp, well-defined ridge just inside the Liki I moraine ridge. Boulders approximately 0.5–1.0 m in diameter are found on the moraine crest. They exhibit limited signs of erosion. We propose an age of $28 \pm 3$ kyr for the landform based on an average of the zero erosion boulder ages. This age agrees well with previous estimates of 30 kyr from paleosols on a correlative moraine in Teleki Valley.

Liki IIA moraines are preserved as several small loops, just inside the limits of the massive Liki II moraine. They are extremely bouldery, have little topographic relief and are very well-preserved. Samples of two boulders yield an average exposure age of $14.6 \pm 1.2$ kyr. Additional samples were collected from large boulders and polished bedrock surfaces just beyond the Liki III limits in Upper Gorges Valley. These surfaces are about 5 km from the Liki IIA moraines and give an average exposure age of $13.0 \pm 2$ kyr. The two bedrock samples give a slightly older age of $17.4 \pm 1.1$ kyr which we attribute to insufficient removal of previously exposed bedrock material. The ages of the erratics should record the minimum time of deglaciation for the surface on which they are located. From the age of the terminal Liki IIA moraine (14.6 kyr), the age of the glacial erratics (13.0 kyr) and the distance between the two, we calculate an average rate of glacier retreat (3 m yr$^{-1}$) during the last deglaciation.

The Naro Moru till is preserved as an isolated deposit containing large boulders (1.0–2.0 m diameter). Based on paleomagnetic information, Mahaney [1] interpreted this till as the remnant of a very old glaciation ($< 730$ kyr). Exposure ages for eight boulders range from 33 kyr to 101 kyr. Like the Liki II deposits in Teleki Valley, this distribution of ages is surprising for a landform in this age range, especially in light of its apparently excellent preservation. Interpretation

of the till is further complicated by its stratigraphic relationship to the Liki I and Liki II deposits. The Naro Moru till is located on the top of a ridge, tens of meters above both of these units. It seems difficult for ice to have deposited till on such a high ridge without obliterating the older and smaller Liki I moraine. Additional field investigations are needed to provide a more accurate interpretation of this landform in terms of its stratigraphy and chronology.

The Gorges moraines located at 2850 m have been interpreted as the oldest and most extensive glacial landform preserved on Mt. Kenya [1]. Based upon lithologic characteristics and remnant magnetization, these moraines are considered to be older than 2.4 Myr [1]. However, the sharp relief and steep slopes of these landforms seem unlikely for a moraine of such age. We sampled the only four boulders we could find on the crest of the landform. These boulders have relatively fresh surfaces but are small (less than 0.5 m in diameter). The landform yields an average exposure age of $6.5 \pm 0.9$ kyr. Based upon its stratigraphic position, this landform cannot be of glacial origin if this age is correct. However, the potential for prior soil cover of these boulders is high because they are so small. A 2.5 m deep soil pit dug into the crest of the landform showed deposits of well-sorted fine sand and silt with no gravel, cobble or boulder fractions and little to no development of soil horizons. These results further support the hypothesis that the Gorges landform is not glacial.

### 4.3. Kilimanjaro, Mawenzi Peak

On the southwest slopes of Mawenzi Peak and the southeast edge of the Saddle, moraines ascribed to the Fourth and the Little Glaciations were identified and sampled. Boulders were also sampled from in front of the Main Glaciation moraines and from the previously reported limits of the Third Glaciation (ca. 3000 m). Moraine and sample locations are indicated in Fig. 3b–d.

The Third Glaciation is considered the most extensive glaciation on Kilimanjaro, based upon reports of boulder beds at 4000 m and glacial striae at 3000 m. Based on the age of volcanic clasts present in the boulder bed, the glaciation is believed to have occurred between 120 and 150 kyr [2]. We identified and sampled a number of rounded boulders that we attributed to the Third Glaciation based upon their position beyond the Fourth Glaciation limits. We also collected a boulder and bedrock pair from 3000 m, the previously estimated limit of the Third Glaciation. The boulders ranged between 0.5 and 3.0 m diameter and exhibited signs of intense weathering and erosion. The bedrock sample gives an infinite age of $> 660$ kyr and is assumed to have prior exposure. As with the Liki II deposits, the high coefficient of variation for the boulder ages (0.49) indicates that extensive soil erosion has occurred and cannot be modeled accurately. We tentatively choose the maximum boulder age (360 kyr) as a minimum age for the landform. Since this age is beyond previous estimates for the Third Glaciation, it is possible that we may have sampled boulders from an older episode such as the First (ca. 500 kyr) or the Second ($> 360$–240 kyr).

On the southern slopes of Mawenzi, moraines of the Main Glaciation are up to 30 m high and several kilometers long. Numerous well-rounded and well-preserved boulders up to 3.0 m in diameter litter the crests of the moraines. Previous attempts to date these deposits have failed because of the lack of datable material [44]. However, an estimate of 10–70 kyr has been based on weathering and relative position [2]. Five boulders collected from these surfaces yield an average surface exposure age of $21 \pm 4$ kyr, indicating that these deposits were emplaced at the last glacial maximum (LGM). Although the standard deviation is large, it is greatly affected by one young (MP-90, 16.4 kyr) and one old (MP-89, 28 kyr) outlier. Using only the other three boulders gives a similar mean age (20 kyr), but with a greatly reduced standard deviation (0.7 kyr).

A complex of moraines southwest of Mawenzi Peak have been ascribed to the Fourth and the Little Glaciations. Based upon their proximity to the moraines of the Main Glaciation, the age of these deposits has been previously estimated at 8–10 kyr [2]. Using aerial photographs and limited field investigations, these moraines were interpreted as a juxtaposition of landforms produced

by the two glacial episodes. The two outermost lateral moraines were ascribed to the Fourth Glaciation. A series of smaller recessional moraines inside these were attributed to the Little Glaciation. All of the surfaces are bouldery and appeared young and well-preserved. We collected samples from the left lateral moraine and from several of the recessional moraines of the Little Glaciation. The boulders give a surprisingly large spread in surface exposure ages, considering the ages of the landforms. The average exposure age for the outer moraine is $16.3 \pm 1.9$ kyr. The inner moraines yield an average age of $15.8 \pm 2.5$ kyr. These ages are statistically indistinguishable because of the large spread in the boulder ages from the individual landforms.

### 4.4. Kilimanjaro, Kibo Peak

On the eastern slopes of Kibo Peak, two distinct moraine loops were identified in the field and on aerial photographs. Boulders appeared unweathered, angular and range from 1.0 to 2.0 m in diameter. In places, boulders were observed directly on striated bedrock surfaces. We collected four boulder samples and three striated bedrock samples. The boulders yield an average age of $13.8 \pm 2.3$ kyr and the bedrock samples give an older age of $23 \pm 5$ kyr. Previous studies [19,45] have shown that bedrock surfaces are likely to give older apparent ages because of prior exposure to cosmic rays. The boulder ages are therefore considered a more reliable estimate of the age of the surface.

### 4.5. Kilimanjaro, Saddle

We collected two samples from large boulders present on the Saddle between Mawenzi and Kibo Peaks. The first boulder, which was approximately 1.5 m diameter and only slightly weathered, gave an age of 38 kyr. The second boulder was larger (3.0 m) but heavily weathered. It gave a significantly younger age of 6.9 kyr. This result was discounted because of the evidence of spalling of the boulder. Major element analysis of both boulders indicates that they were derived from Mawenzi Peak. We propose that this boulder train was formed by ice flowing from Mawenzi Peak before 40 kyr when the coalesced Kibo and Mawenzi ice masses broke up and the Saddle was deglaciated.

### 4.6. Calculated soil erosion rates for glacial moraines

The newly developed soil–boulder erosion model permits the estimation of soil erosion rates for glacial landforms. Table 3 displays the soil erosion rates calculated for the Liki I and the Teleki moraines on Mt. Kenya. The older, but steeper, Liki I moraine yields soil erosion rates that are twice those of the younger, subdued Teleki moraine. These results may reflect the wetter climate in Teleki Valley (Teleki moraine) on the western slopes of the mountain compared with the arid, eastern Gorges Valley (Liki I). These preliminary estimates offer intriguing possibilities for future applications of cosmogenic isotopes to the rates of landscape evolution.

## 5. Summary and conclusions

New cosmogenic $^{36}$Cl ages for the glacial deposits of Mt. Kenya and Kilimanjaro permit the development of an improved chronology for glaciations in equatorial East Africa during the Quaternary. These results provide important new information about the timing of climate change in equatorial regions where terrestrial data are scarce. The revised composite chronology of glaciations from both mountains is displayed in Fig. 8.

The most extensive glaciation in equatorial East Africa occurred before 360 kyr ago, based upon cosmogenic ages of heavily weathered deposits on Kilimanjaro. Although bedrock gives an age of

Table 3
Erosion rates of moraine crests

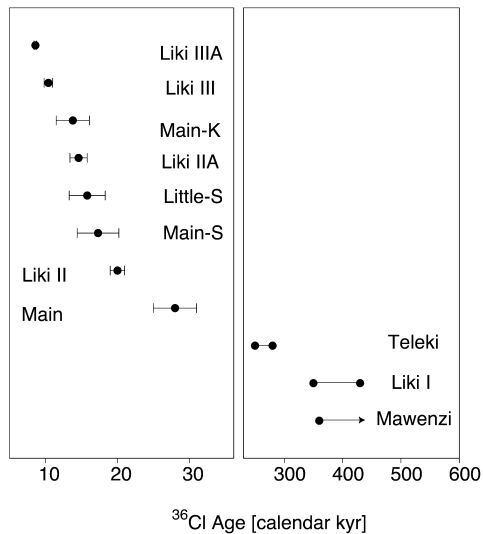| Moraine | Age (kyr) | Coefficient of variation | Soil erosion rate (mm kyr$^{-1}$) |
| --- | --- | --- | --- |
| Teleki | 254–284 | 0.247 | 15.1–17.8 |
| Liki I | 353–419 | 0.135 | 5.2–6.7 |

Fig. 8. Compilation of cosmogenic $^{36}$Cl ages for East African glaciations.

660 kyr, it is not clear that this bedrock age represents the age of a glacial episode because of complications with erosion and prior exposure. The oldest deposits sampled on Mt. Kenya (355–420 kyr) indicate that the oldest glaciations on both mountains may be correlative. This age range may correspond to either oxygen isotope stage (OIS) 10 or 12 depending upon the rate of boulder and soil matrix erosion.

The age of the Teleki deposits (255–285 kyr) indicates that they correlate with marine OIS 8. Interestingly, the elevation of the Teleki moraine is approximately 500 m lower than the older Liki I deposits on the eastern slopes of Mt. Kenya. Either the correlative Liki I deposits in Teleki Valley were at lower elevations on the western side of Mt. Kenya than on the eastern side, and were not preserved, or paleoclimate changes manifested themselves differently on the eastern and western slopes of Mt. Kenya.

Few terrestrial paleoclimate records extend as far back as 400 kyr. For this reason alone, the recognition of glacial deposits in the tropics correlative with OIS 8 and 10 is a significant finding. Combined with the apparent lack of deposits correlative with OIS 6, this result is especially intriguing. The absence of stage 6 deposits indicates that either they were not deposited at all or that

they were obliterated by more extensive, younger glacial advances. This is in contradiction to what has typically been inferred about the relative extent of stage 6 from glacial deposits at high latitudes [46–48]. Furthermore, $\delta^{18}$O in marine sediments (a proxy for sea level and ice volume) [49] and $\delta^{18}$O$_{atm}$ in ice cores (a proxy for temperature) [50] both indicate that OIS 6 was larger than OIS 8. However, the record of $\delta^{18}$O in calcite from Devils Hole, NV, USA [51], appears to agree well with the data from East African moraines: OIS 10 is large, OIS 8 is slightly smaller and OIS 6 is significantly smaller than both of these episodes. The significance of these results is unclear in particular because of the lack of other proxy records for this time period. However, they may indicate that the low-latitude climate response at this time became decoupled from that at higher latitudes, a result which may be critical to evaluating the relative importance of high- and low-latitude sites in the forcing of major climate shifts.

Our $^{36}$Cl ages indicate that a series of younger advances occurred at $28 \pm 3$, $20 \pm 1$, between $15.8 \pm 2.5$ and $13.8 \pm 2.8$, $10.4 \pm 0.6$ and possibly at $8.6 \pm 0.5$ kyr. This record of glaciations agrees strongly with the results of other studies in East Africa. Reconstructions of temperature and precipitation for the last 40 kyr using pollen records indicate that Africa was cold and dry between ca. 35 and 15 kyr [52]. Sedimentary and diatom records confirm that lake levels were low during this interval, with the driest period occurring at around 21 kyr [53], the time when the moraines of the Main Glaciation were deposited on Kilimanjaro. The end of this cold, dry period was punctuated by a sharp increase in temperature and precipitation to present values at around 15 kyr [52]. This age is in agreement with the time of glacial retreat from the LGM glacial limits ($15.8 \pm 2.5$ to $13.8 \pm 2.8$), within the uncertainties in both the pollen and glacial chronologies. Prior to this abrupt climate shift, the pollen record is characterized by 3–4°C fluctuations in temperature around a mean which was $4 \pm 2$°C lower than today [52]. Pollen data also indicate large variability in precipitation during this time, which is corroborated by the lake level record of fluctuations between dry and wet periods at ca. 14–18

kyr [54,64]. These variations in temperature and precipitation are consistent with the record of multiple glacial advances and retreats just inside the LGM ice limit.

Following a period of high lake levels, an episode of strong aridity is recorded across East Africa at 13–11 cal. kyr [32,54–57], which has been correlated with the European Younger Dryas cold interval. The Liki III readvance $(10.2 \pm 0.5)$ in the upper valleys of Mt. Kenya appears to post-date this climate episode. However, correlation with the Younger Dryas event cannot be ruled out until the systematic errors involved in our geomagnetic correction are better understood.

The final glacial event, at $8.6 \pm 0.5$ kyr, may correspond to an early Holocene cold event recorded elsewhere between 8.4 and 8.0 kyr [58,59]. If accurate, this age would indicate that glaciers on Mt. Kenya respond to century scale climatic shifts. However, this age is uncertain and stronger evidence is needed to confirm this hypothesis.

The results of this study provide a unique record of climate change in tropical East Africa. Few other long-term records of climate change in Africa have been identified. Most of the records which extend further than 100 kyr are based upon pollen and mineralogical studies of marine cores [60–63]. These records clearly indicate that the glacial periods corresponding to even-numbered marine OISs were cool and dry, whereas the interglacial periods were warm and humid. Numerous short-term records of climate derived from lake levels [56] and from pollen [52,64] confirm these results for the last 50 kyr. The new chronology of glacial fluctuations in equatorial East Africa lends additional support to the variability of tropical climates during the Quaternary and hints at the possibility of links between low- and high-latitude climate changes.

## Acknowledgements

## References

[1] W.C. Mahaney, Ice on the Equator: Quaternary Geology of Mount Kenya, East Africa, Wm Caxton, 1990, 398 pp.

[2] C. Downie and P. Wilkinson, The Geology of Kilimanjaro, University of Sheffield, Sheffield, 1972, 253 pp.

[3] S. Hastenrath, The Glaciers of Equatorial Africa, Reidel, 1984, 353 pp.

[4] R.W. Barendregt, W.C. Mahaney, Paleomagnetism of selected Quaternary sediments on MT Kenya, East Africa a reconnaissance study, J. Afr. Earth Sci. 7 (1988) 219–225.

[5] W.C. Mahaney, Holocene glaciations and paleoclimate of Mount Kenya and other East Africa mountains, Quat. Sci. Rev. 7 (1988) 211–225.

[6] D. Elmore, F.M. Phillips, Accelerator mass spectrometry for measurement of long-lived radioisotopes, Science 236 (1987) 543–550.

[7] P.J. Aruscavage, E.Y. Campbell, An ion-selective electrode method for determination of chlorine in geological materials, Talanta 30 (1983) 745–749.

[8] T.E. Cerling, H. Craig, Geomorphology and in-situ cosmogenic isotopes, Annu. Rev. Earth Planet. Sci. 22 (1994) 273–317.

[9] D. Lal, Cosmic ray labeling of erosion surfaces in situ nuclide production rates and erosion models, Earth Planet. Sci. Lett. 104 (1991) 424–439.

[10] P.R. Bierman, K.A. Marsella, C. Patterson, P.T. Davis, M. Caffee, Mid-Pleistocene cosmogenic minimum-age limits for pre-Wisconsinan glacial surfaces in southwestern Minnesota and southern Baffin island a multiple nuclide approach, Geomorphology 27 (1–2) (1999) 25–39.

[11] E.J. Brook, M.D. Kurz, J.R.P. Ackert, Chronology of Taylor Glacier advances in Arena Valley, Antarctica, using in situ cosmogenic $^3$He and $^{10}$Be, Quat. Res. 39 (1993) 11–23.

[12] E.J. Brook, E.T. Brown, M.D. Kurz, J.R.P. Ackert, G.M. Raisbeck, F. Yiou, Constraints on age, erosion, and uplift of Neogene glacial deposits in the Transantarctic Mountains determined from in situ cosmogenic $^{10}$Be and $^{26}$Al, Geology 23 (12) (1995) 1063–1066.

[13] J.C. Gosse, J. Klein, E.B. Evenson, B. Lawn, R. Middleton, Beryllium-10 dating of the duration and retreat of the last Pinedale glacial sequence, Science 268 (1995) 1329–1333.

[14] J.C. Gosse, E.B. Evenson, J. Klein, B. Lawn, R. Middleton, Precise cosmogenic $^{10}$Be measurements in western North America Support for a global Younger Dryas cooling event, Geology 23 (1995) 877–880.

[15] F.M. Phillips, M.G. Zreda, S.S. Smith, D. Elmore, P.W. Kubik, P. Sharma, A cosmogenic chlorine-36 chronology for glacial deposits at Bloody Canyon, Eastern Sierra Nevada, California, Science 248 (1990) 1529–1532.

[16] F.M. Phillips, M.G. Zreda, M.A. Plummer, L.V. Benson, D. Elmore, P. Sharma, Chronology for fluctuations in Late Pleistocene Sierra Nevada glaciers and lakes, Science 274 (5288) (1996) 749–751.

[17] F.M. Phillips, M.G. Zreda, J.C. Gosse, J. Klein, E.B. Evenson, R.D. Hall, O.A. Chadwick, P. Sharma, Cosmogenic $^{36}$Cl and $^{10}$Be ages of Quaternary glacial and fluvial deposits of the Wind River Range, Wyoming, Geol. Soc. Am. Bull. 109 (11) (1997) 1453–1463.

[18] M.G. Zreda, F.M. Phillips, Insights into alpine moraine development from cosmogenic $^{36}$Cl buildup dating, Geomorphology 14 (2) (1995) 149–156.

[19] M. Zreda, J. England, F. Phillips, D. Elmore, P. Sharma, Unblocking of the Nares Strait by Greenland and Ellesmere ice-sheet retreat 10 000 years ago, Nature 398 (1999) 139–142.

[20] M.G. Zreda and F.M. Phillips, Surface exposure dating by cosmogenic chlorine-36 accumulation, in: C. Beck (Ed.), Dating in Exposed and Surface Contexts, University of New Mexico Press, 1994, pp. 161–183.

[21] B. Liu, F.M. Phillips, J.T. Fabryka-Martin, M.M. Fowler, R.S. Biddle, Cosmogenic $^{36}$Cl accumulation in unstable landforms. 1. Effects of the thermal neutron distribution, Water Resour. Res. 30 (11) (1994) 3115–3125.

[22] F.M. Phillips, M.A. Plummer, CHLOE A program for interpreting in-situ cosmogenic nuclide data for surface exposure dating and erosion studies, Radiocarbon 38 (1996) 98.

[23] F.M. Phillips, M.G. Zreda, M.R. Flinsch, D. Elmore, P. Sharma, A reevaluation of cosmogenic $^{36}$Cl production rates in terrestrial rocks, Geophys. Res. Lett. 23 (9) (1996) 949–952.

[24] T. Swanson, Determination of $^{36}$Cl production rates from the deglaciation history of Whidbey and Fidalgo Islands, Washington, Radiocarbon 38 (1996) 172.

[25] J.O. Stone, G.L. Allan, L.K. Fifield, R.G. Cresswell, Cosmogenic chlorine-36 from calcium spallation, Geochim. Cosmochim. Acta 60 (1996) 679–692.

[26] Y. Guyodo, J.P. Valet, Relative variations in geomagnetic intensity from sedimentary records: The past 200 000 years, Earth Planet. Sci. Lett. 143 (1–4) (1996) 23–36.

[27] D. Lal and B. Peters, Cosmic ray produced radioactivity on earth, in: K. Sitte (Ed.), Encyclopedia of Physics: Cosmic Rays II, Encyclopedia of Physics 46/2, Springer-Verlag, Berlin, 1967, pp. 551–612.

[28] W. Elsaesser, E.P. Ney, J.R. Winckler, Cosmic-ray intensity and geomagnetism, Nature 178 (1956) 1226–1227.

[29] E. Tric, J.-P. Valet, P. Tucholka, M. Paterne, L. Labeyrie, F. Guichard, L. Tauxe, Paleointensity of the geomagnetic field during the last 80 000 years, J. Geophys. Res. 97 (1991) 9337–9351.

[30] M. Frank, B. Schwarz, S. Baumann, P.W. Kubik, M. Suter, A. Mangini, A 200 kyr record of cosmogenic radionuclide production rate and geomagnetic field intensity from Be-10 in globally stacked deep-sea sediments, Earth Planet. Sci. Lett. 149 (1–4) (1997) 121–129.

[31] M. Stuiver, P. Reimer, E. Bard, G. Burr, K. Hughen, B. Kromer, G. McCormac, J.V.d. Plicht, INTCAL98 radiocarbon age calibration, 24 000–0 cal BP, Radiocarbon 40 (3) (1998) 1041–1083.

[32] C. Hillaire-Marcel, O. Carro, J. Casanova, $^{14}$C and Th/U dating of Pleistocene and Holocene stromatolites from East African paleolakes, Quat. Res. 25 (1986) 312–329.

[33] M. Servant, M. Fournier, J. Argollo, S. Servantvildary, F. Sylvestre, D. Wirrmann, J.P. Ybert, The last glacial interglacial transition in the south tropical Andes (Bolivia) based on comparisons of lacustrine and glacial fluctuations, Comptes Rendus Acad. Sci.-Serie II 320 (8) (1995) 729–736.

[34] J.D. Clayton, C.M. Clapperton, Broad synchrony of a late-glacial glacier advance and the highstand of palaeolake Tauca in the Bolivian Altiplano, J. Quat. Sci. 12 (3) (1997) 169–182.

[35] M.D. Kurz, D. Colodner, T.W. Trull, R.B. Moore, K. O'Brien, Cosmic ray exposure dating with in situ produced cosmogenic $^{3}$He: Results from young lava flows, Earth Planet. Sci. Lett. 97 (1990) 177–189.

[36] P. Sarda, T. Staudacher, C.J. Allègre, A. Lecomte, Cosmogenic neon and helium at Réunion measurement of erosion rate, Earth Planet. Sci. Lett. 119 (1993) 405–417.

[37] J.E.T. Channell, D.A. Hodell, B. Lehman, Relative geomagnetic paleointensity and $\delta^{18}$O at ODP Site 983 (Gardar Drift, North Atlantic) since 350 ka, Earth Planet. Sci. Lett. 153 (1997) 103–118.

[38] J. Brassart, E. Tric, J.P. Valet, E. Herrero-Bevera, Absolute paleointensity between 60 and 400 ka from the Kohala mountain (Hawaii), Earth Planet. Sci. Lett. 148 (1997) 141–156.

[39] R. Braucher, F. Colin, E. Brown, D. Bourles, O. Bamba, G. Raisbeck, F. Yiou, J. Koud, African laterite dynamics using in situ-produced Be-10, Geochim. Cosmochim. Acta 62 (9) (1998) 1501–1507.

[40] H. Cockburn, M. Seidl, M. Summerfield, Qualifying denudation rates on inselbergs in the central Nambin Desert using in situ-produced cosmogenic Be-10 and Al-26, Geology 27 (5) (1999) 399–402.

[41] R. Braucher, D. Bourles, F. Colin, E. Brown, B. Boulange, Brazilian laterite dynamics using in situ-produced Be-10, Earth Planet. Sci. Lett. 163 (1–4) (1998) 197–205.

[42] M.G. Zreda, F.M. Phillips, D. Elmore, Cosmogenic $^{36}$Cl accumulation in unstable landforms, 2. Simulations and

measurements on eroding moraines, Water Resour. Res. 30 (1994) 3127–3136.

[43] R.E. Taylor, M. Stuiver, P.J. Reimer, Development and extension of the calibration of the radiocarbon time scale archeological applications, Quat. Sci. Rev. 15 (1996) 655–668.

[44] H. Osmaston, Glaciers, glaciation and equilibrium line altitudes on Kilmanjaro, in: W.C. Mahaney (Ed.), Quaternary and Environmental Research on East African Mountains, A.A. Balkema, Rotterdam, 1989, p. 483.

[45] J.P. Briner, T.W. Swanson, Using inherited cosmogenic $^{36}$Cl to constrain glacial erosion rates of the Cordilleran ice sheet, Geology 26 (1998) 3–6.

[46] T. Nilsson, The Pleistocene: Geology and Life in the Quaternary, Ferdinand Enke Verlag, Stuttgart, 1983, 651 pp.

[47] J. Ehlers, Quaternary and Glacial Geology, Wiley, Chichester, 1996, 578 pp.

[48] R.F. Flint, Glacial and Quaternary Geology, John Wiley and Sons, New York, 1971, 892 pp.

[49] N.J. Shackleton, Oxygen isotopes, ice volume and sea-level, Quat. Sci. Rev. 6 (3–4) (1987) 183–190.

[50] J.R. Petit, J. Jouzel, D. Raynaud, N.I. Barkov, J.M. Barnola, I. Basile, M. Bender, J. Chappellaz, M. Davis, G. Delaygue, M. Delmotte, V.M. Kotlyatov, M. Legrand, V.Y. Lipenkov, C. Lorius, L. Pepin, C. Ritz, Climate and atmospheric history of the past 420 000 years from the Vostok ice core, Antarctica, Nature 399 (1999) 429–435.

[51] I.J. Winograd, J.M. Landwehr, K.R. Ludwig, T.B. Coplen, A.C.R. AC, Duration and structure of the past four interglaciations, Quat. Res. 48 (2) (1997) 141–154.

[52] R. Bonnefille, J.C. Roeland, J. Guiot, Temperature and rainfall estimates for the past 40 000 years in equatorial Africa, Nature 346 (1990) 347–349.

[53] F. Gasse, V. Lédée, M. Massault, J.C. Fontes, Water-level fluctuations of Lake Tanganyika in phase with oceanic changes during the last glaciation and deglaciation, Nature 342 (6245) (1989) 57–59.

[54] R. Bonnefille, G. Riollet, G. Buchet, M. Icole, R. Lafont, M. Arnold, D. Jolly, Glacial/interglacial record from intertropical Africa, high resolution pollen and carbon data at Rusaka, Burundi, Quat. Sci. Rev. 14 (1995) 917–936.

[55] M. Servant, J. Maley, B. Turcq, M.L. Absy, P. Brenac, M. Fournier, M.P. Ledru, Tropical forest changes during the late Quaternary in African and South American lowlands, Glob. Planet. Change 7 (1993) 25–40.

[56] N. Roberts, M. Taieb, P. Barker, B. Damnati, M. Icole, D. Williamson, Timing of the Younger Dryas event in East Africa from lake-level changes, Nature 366 (6451) (1993) 146–148.

[57] F.A. Street-Perrott and N. Roberts, Fluctuations in closed-basin lakes as an indicator of past atmospheric circulation patterns, in: A. Street-Perrott, M. Beran and R. Ratcliffe (Eds.), Variations in the Global Water Budget, D. Reidel, Boston, 1983, pp. 331–345.

[58] R.B. Alley, P.A. Mayewski, T. Sowers, M. Stuiver, K.C. Taylor, P.U. Clark, Holocene climatic instability: a prominent, widespread event 8200 yr ago, Geology 25 (6) (1997) 483–486.

[59] S.R. O'Brien, P.A. Mayewski, L.D. Meeker, M.S. Twickler, S.I. Whitlow, Complexity of Holocene climate as reconstructed from a Greenland ice core, Science 270 (1995) 1962–1964.

[60] S. Jahns, M. Huls, M. Sarnthein, Vegetation and climate history of west equatorial Africa based on a marine pollen record off Liberia (site GIK 16776) covering the last 400 000 years, Rev. Palaeobot. Palynol. 102 (3–4) (1998) 277–288.

[61] F.X. Gingele, P.M. Muller, R.R. Schneider, Orbital forcing of freshwater input in the Zaire Fan area-clay mineral evidence from the last 200 kyr, Palaeogeogr. Palaeoclimatol. Palaeoecol. 138 (1–4) (1998) 17–26.

[62] T.C. Partrige, Warming phases in Southern Africa during the last 150 000 years an overview, Palaeogeogr. Palaeoclimatol. Palaeoecol. 101 (1993) 237–244.

[63] H. Hooghiemstra, H. Stalling, C.O.C. Agwu, L.M. Dupont, Vegetational and climatic changes at the northern fringe of the Sahara 250 000–5000 years BP: evidence from 4 marine pollen records located between Portugal and the Canary Islands, Rev. Palaeobot. Palynol. 74 (1992) 1–53.

[64] A. Vincens, F. Chalie, R. Bonnefille, J. Guilot, J.-J. Tiercelin, Pollen-derived rainfall and temperature estimates from Lake Tanganyika and their implication for the Late Pleistocene water levels, Quat. Res. 40 (1993) 343–350.